Chapter 4

Effect of addition of NK75 nanoclay on properties of PET/clay nanohybrid

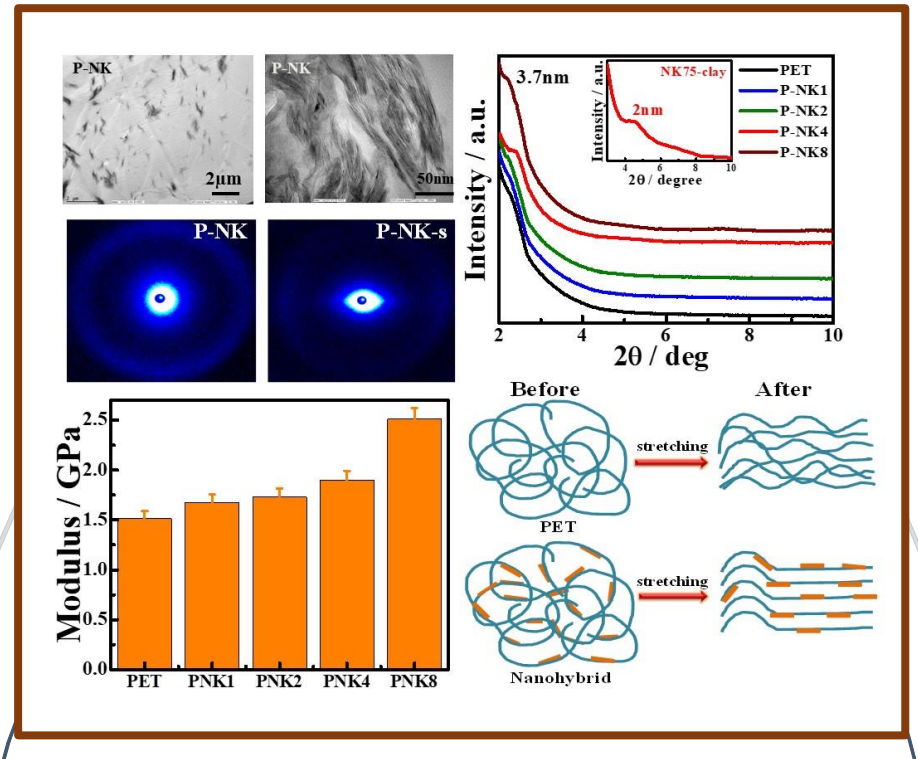

Chapter 4

4.1 Introduction

The polymer nanocomposites have emerged in past decades and have shown betterment in various properties at comparatively very low filler loading due to the large surface area of fillers. As discussed in the first chapter, the large surface area of nanoclays provides more interactions of nanofillers and polymer matrix in polymer nanohybrids. The factors which play major role to improve the properties of the nanocomposites are homogeneous dispersion of the filler material in the matrix, intercalation of matrix material into filler material, exfoliation of the filler and strong interaction between filler and matrix material. These factors result into improvement of various properties such as mechanical, thermal, gas barrier etc. [1, 16, 91, 92, 94, 98, 101, 106, 108, 109, 164, 170-172, 187, 222-231].

In the present chapter, the preparation of polymer nanohybrid in order to enhance its properties have been done using NK75 nanoclay. NK75 is an Indian origin nanoclay which is a modified montmorillonite clay having a repeating planar 2:1 layered silicate structure where planar octahedral alumina layer is sandwiched between two tetrahedral silicate layers (structure has been shown in ***Chapter 1***, ***Figure 1.12***) [222]. It has high amount of iron in it which makes it biocompatible and viable for the biomedical applications [224]. It has cation exchange capacity (CEC) of 70 mequiv. per 100g and ion exchanged with dimethyl dihydrogenated tallow ammonium. The structure of organic modifier has been shown in ***Figure 4.1***.

Most of the fillers, upon consolidating in the polymer, incorporate brittleness in the nanocomposites and reduces toughness and elongation at break conspicuously which is not desirable [92]. Thus, a balance among various properties according to the specific application

is achieved by modulating the various factors. Frounchi and Dourbash [109] prepared PET nanohybrids with Nanolin DK2 and Cloisite 15A clays using melt processing technique and observed the effect of dispersion of clay on morphology and permeability of the PET/clay nanohybrids with the amount of filler content. The elastic modulus was improved slightly whereas gas barrier properties were improved up to 30% at 3 wt % clay loading. Clay concentration of 2% decreased elongation at break by ~60% whereas more than 2% clay concentration hindered processability in Nanolin DK2 clay nanocomposites as injection molding could not be possible. 3% clay concentration decreased elongation at break by ~80% in nanocomposites using Cloisite 15A as well.

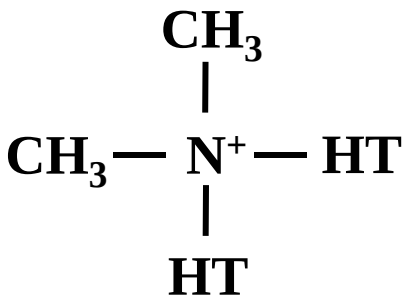

Figure 4.1: *Structure of organic modifier which is used for modification of NK75. HT denotes hydrogenated tallow, which contains ~65% C_{18}, ~30% C_{16}, ~5% C_{14}.*

Pandey et al. [16] prepared thermoplastic polyurethane (TPU) nanocomposites using NK75 nanoclay and studied the effect of nanoclay on mechanical and gas barrier properties. The nanoclay was found to be homogeneously dispersed and intercalated in the TPU polymer matrix. The mechanical properties were improved as Young's modulus increased 33% for 4 wt% and 66% for 10 wt% clay concentration respectively. The toughness retained and increased up to 4 wt% of NK75 clay concentration whereas more clay content resulted in toughness decrement. The nitrogen gas permeability decreased and nanohybrids were found

to have improved gas barrier properties. NK75 nanoclay was used by Kapusetti et al. [224] to develop nanohybrids of PMMA based bone cement. The mechanical properties such as modulus and toughness were improved significantly along with improvement in other properties.

In this study, nanohybrids of PET with nanoclay (NK75) have been prepared via solution route. The effect of nanoclay on stretching, structural development, mechanical and gas barrier properties has been studied thoroughly and verified with theoretical models. The interaction and dispersion of nanoclay with polymer matrix have been inspected and the nanohybrids have been tested showing significant property development. The experimental results have been predicted via different models using various fitting parameters.

4.2 Experimental

Materials: PET, NK75 nanoclay, DCM

Preparation of nanohybrid: Nanohybrids of PET and NK75 clay have been prepared through solvent casting route as explained in ***Chapter 2***. PET nanohybrids have been abbreviated as P-NK1, P-NK2, P-NK4, P-NK8 for 1, 2, 4 and 8 weight percentage of nanoclay concentration respectively. Abbreviation P-NK have been used for the 4% of clay concentration.

4.3 Results and discussion

4.3.1 Dispersion and interactions

The structure of nanohybrid has nanoclay platelets dispersed in the PET matrix. To study the level of dispersion, the TEM studies were done.

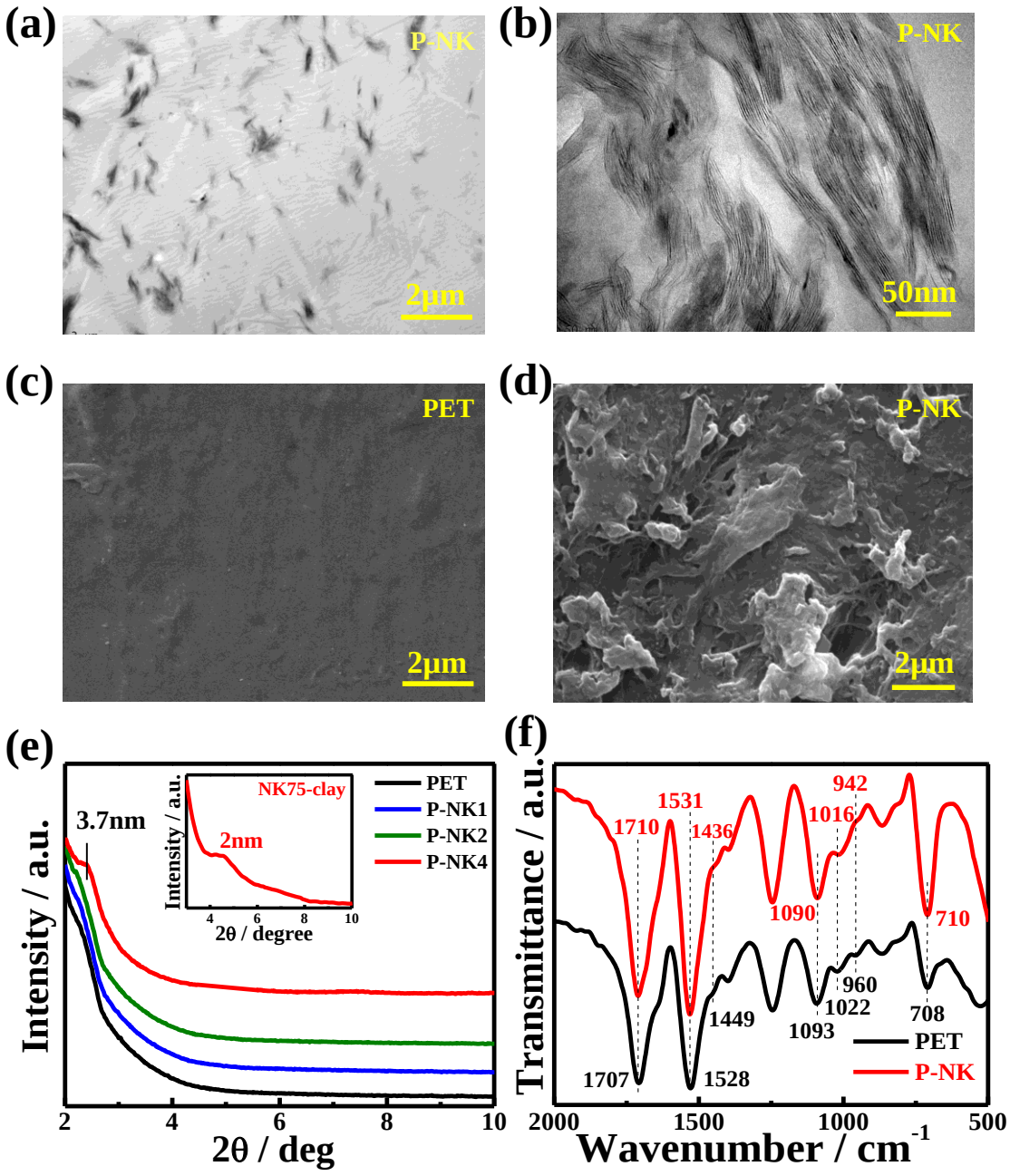

Figure 4.2: *TEM micrograph of nanohybrid,* ***(a)*** *lower magnification (left image) and* ***(b)*** *high magnification image (right side image) shows the intercalated pattern for 4% clay content nanohybrid; SEM images of* ***(c)*** *PET and* ***(d)*** *P-NK;* ***(e)*** *Wide-angle XRD patterns of PET and nanohybrid, inset figure shows the XRD pattern of pure nanoclay; and* ***(f)*** *FTIR spectra of neat PET and P-NK containing 4% of NK75 nanoclay.*

The qualitative analysis of organically modified clay distribution throughout the matrix was done by bright field TEM imaging. The result is shown in ***Figure 4.2a***. The TEM image showed the P-NK nanohybrid had a homogeneous distribution of NK75 nanoclay throughout the polymer matrix. In the further magnified TEM image, the platelets of nanoclay could be seen to have an intercalated structure (***Figure 4.2b***). The platelets had evidently increased intergallery spacing. It could be seen that the nanoclay particles had some amount of agglomeration. The complete elimination of agglomeration is not practically possible. Although it enhances the material's rigidity to an extent but also causes degradation in other mechanical properties such as ductility, elongation at break and mechanical strength. The average aspect ratio (ratio of length to thickness) was calculated by measuring the length and the thickness of nanoclay particles. The average aspect ratio was calculated to be 20. The nanoparticles were dispersed in the matrix in form of tactoids which had an intercalated structure. The average correlation length was estimated to be 315nm [171, 172]. To investigate the surface morphology of P-NK nanohybrids, SEM study was done. The pure polymer PET showed smooth surface whereas the P-NK nanohybrid showed roughened surface morphology because of the presence of nanoclay particles as shown in ***Figure 4.2c*** and ***d***.

XRD plots of pure PET and P-NK nanocomposite are shown in ***Figure 4.2e***. The pure PET did not show any strong peak. The nanohybrids with lower concentrations of clay did not show any peak whereas the P-NK nanohybrid had a strong reflection peak at $2\theta = 2.37°$. This peak signifies an interplanar distance of 3.7nm corresponding (d_{001}) plane. The XRD of pure P-NK (inset image of ***Figure 4.2e***) showed the characteristic interplanar distance of

organically modified NK75 as 2 nm. The increment of intergallery spacing or interplanar distance was due to the intrusion of polymer chain between the clay platelets resulting intercalation in nanohybrid. The increased d-spacing causing increased level of interaction because of the strong interaction of polymer and nanoclay particles. The nanohybrids containing lower clay concentrations do not show distinct reflection peak due to the presence of less clay platelets resulting in lower coherency.

FTIR has been performed on pure PET and its nanohybrids (P-NK) to understand the nature of interaction (***Figure 4.2f***). The strong peak at 1707 cm^{-1} corresponds to the symmetric stretching of ester bond (-C=O) of PET which is shifted to 1710 cm^{-1} in presence of nanoclay because of strong interaction of clay platelets and polymer. The band at 1528 cm^{-1} is attributed to para substituted benzene ring shifts to 1531 cm^{-1} in nanohybrid. The peaks at 1022 and 708 cm^{-1} are associated to a combination of ring (C-H) in plane, ring (C-H) out of plane and ring (C-C) bending. In presence of clay, these peaks shift to 1016 and 710 cm^{-1}, respectively. The peak shifting from 1093 to 1090 cm^{-1} corresponds to the symmetric glycol (C-O) stretch**.** The absorption band at 2927 cm^{-1} is associated with (–C-H) bond stretching which shifts to 2925 cm^{-1}. The band at 960 cm^{-1} is assigned to trans (O-CH_2) stretching which shifts to 942 cm^{-1} due to interactions with nanoclay particles. The peak at 1449 cm^{-1} corresponds to (CH_2) bending in amorphous phase which shifts to 1436 cm^{-1} in nanohybrid. These considerable shifting of FTIR peaks confirms the good interactions between nanoclay with polymer matrix and explains well the homogeneous dispersion of nanoclay in PET matrix and clearly indicate the expected better properties in nanohybrid [1, 231]. The considerable shifting of FTIR peaks confirms the good interactions between nanoclay with polymer matrix.

4.3.2 Thermal properties and stability

Figure 4.3a shows the TGA patterns where degradation of PET occurs at around 410^{o}C whereas P-NK degrades at 401^{o}C. The thermal stability of the nanohybrid is almost similar with pure PET as observed from the mass loss measurement as a function of temperature. Slightly low temperature of nanohybrids is presumably due to the degradation of clay modifier between the clay sheets at higher temperatures [222]. The glass transition temperature reflects the molecular movement of the polymer chain and its increment in nanohybrid clearly indicate stiffness of the chain in presence of nanoclay. The glass transition temperature is observed to be increased about 8^{o}C in nanohybrid as compared to pure polymer as evident from DTA and DSC thermograms (inset of ***Figure 4.3a*** and ***Figure 4.3b***). The thermal property enhancement in terms of glass transition temperature occurred due to good interaction, presumably arising from interaction between hydrophobic PET and dimethyl dihydrogenated tallow ammonium modified NK75 nanoclay [223].

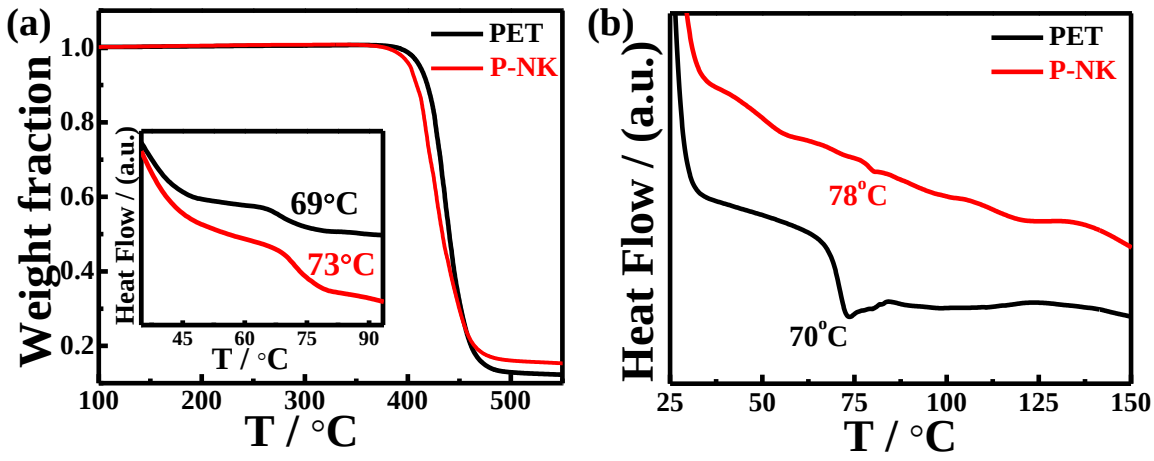

Figure 4.3: (a) *Thermal stability of nanohybrid as compared to pure PET obtained through TGA thermograms. Inset figure shows DTA thermograms; and* ***(b)*** *DSC thermograms showing glass transition temperature of PET and its nanohybrids.*

4.3.3 Mechanical responses and predictions

Figure 4.4a shows the stress-strain curves of PET and its representative nanohybrid. Young's modulus of nanohybrid has increased 66% for 8 wt% nanoclay concentration (***Figure 4.4b***). The increase in modulus is attributed to the formation of a three dimensional superstructure of tactoids after attaining a percolation threshold [91]. The increasing amount of nanoclay results in the restriction of freely rotation of clay tactoids causing enhanced stiffness. Specifically, the mechanical properties of nanohybrids depend on the dispersion, interfacial strength, affinity of components, spatial organization etc. [101]. The nanoparticles work as the entanglement attractors. As the deformation proceeds, they trap and disturb the elementary paths of the polymer chains. This results in the enhanced particle-chain entanglement network [187, 188]. Here, good particle-polymer interaction is taken as the imperative condition for this effect. Moreover, the polymer nanohybrids have the clusters and large tactoids present in the system which can act as the crack propagation centre and, hence, can be the reason of premature breaking of the nanohybrid samples [91]. The modulus increases with increased clay incorporation while the elongation at break reduces slightly as expected because of the increased mechanical rigidity. However, the toughness, as measured from the area under stress-strain curve, exhibits certain reduction having optimum value for 4 wt. % nanoclay containing hybrid (***Figure 4.4c***). The toughness reduction has been observed only 6% for 4wt% of filler concentration and 17% for 8 wt % of filler concentration as compared to pure PET while most of the composite using commercial clay exhibited drastic reduction in toughness, as the elongation at break reduces significantly. The nanohybrids have not shown any considerable brittleness at even higher percentage of clay loadings.

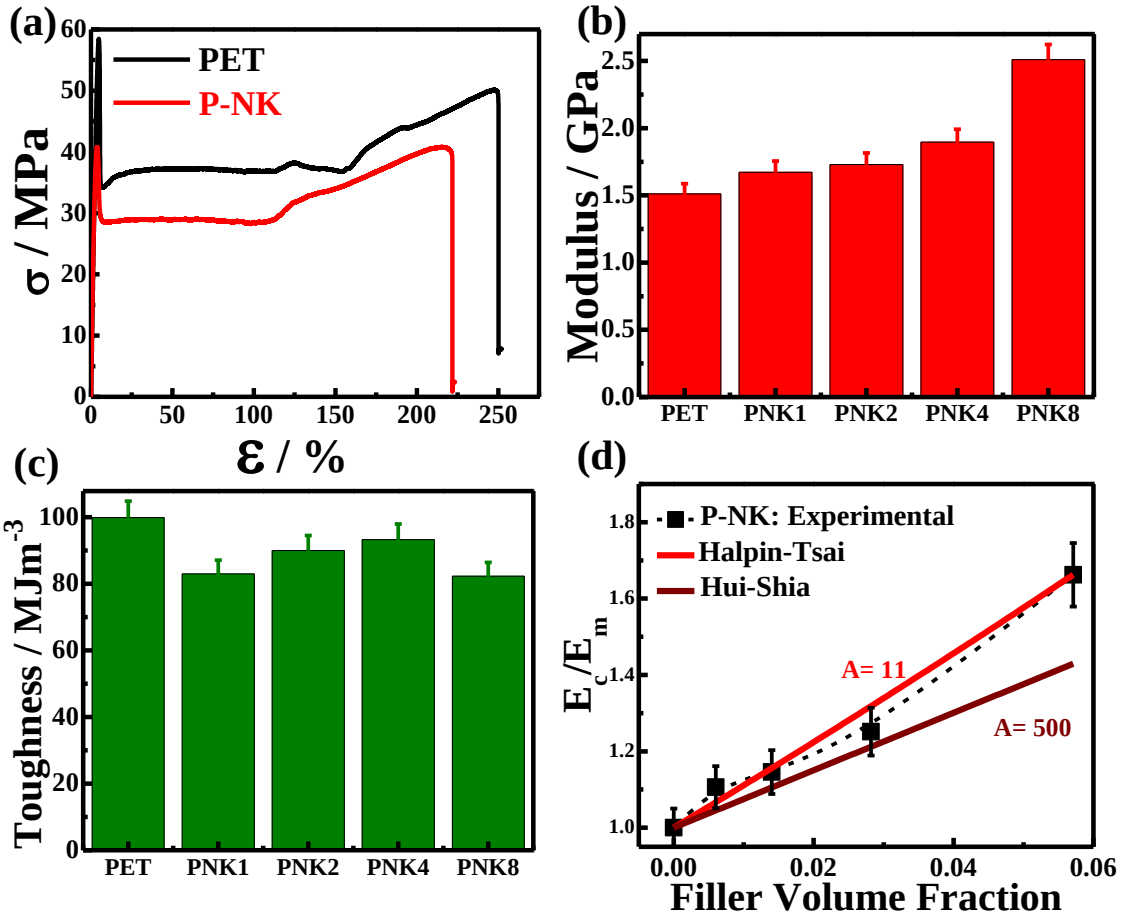

Figure 4.4: ***(a)*** *Stress- strain curves of PET and its nanohybrid (4% nanoclay containing hybrid);* ***(b)*** *Variations of tensile modulus of nanohybrids as a function of nanoclay concentration;* ***(c)*** *Variations of toughness of nanohybrids as a function of nanoclay concentration; and* ***(d)*** *Fitting of elastic modulus – experimental and predicted.*

The mechanical properties have shown better improvement in comparison to previous results with other clays where modulus was shown increasing but with huge toughness reduction in nanocomposites [94, 98]. Almost similar toughness in this nanohybrid is due to the fact that the nanoclay particles have shorter lateral dimension which helps in rotation of the clay particles upon uniaxial stretching. This leads to a better stress transfer and less brittleness in the nanohybrids at even higher clay percentages. The nanoclay has not imparted brittleness

in the nanohybrids whereas most commercial clay reduced brittleness drastically. The toughness retainment is far better than the previously reported data [94, 98, 109].

Halpin Tsai [188] and Hui Shia [190] models have been used for the modulus prediction studies (***Figure 4.4d***). Halpin Tsai model is widely used for the fiber reinforced composites for prediction of tensile modulus as a function of filler volume fraction and aspect ratio. Halpin-Tsai model fits at an aspect ratio of 12. This model predicts the values very closely whereas the Hui-Shia model fits up to 2%. The deviation after that is due to the assumption (perfect interfacial bonding and unidirectional orientation of the filler) which is not the case practically. Here the modulus of the clay has been taken as 200 GPa which can be varied up to 275 GPa [16, 232].

4.3.4 Microhardness of the nanohybrids and predictions

The impressions of diamond indenter show that P-NK has comparatively darker impression due to the presence of nanoclay **(*Figure 4.5a*)**. Microhardness values obtained for the samples are shown in ***Table 4.1***. The hardness increases up to 16% for 8 wt. % of nanoclay. The increase in hardness of the nanohybrid depends on the strong bonding of the filler particles with polymer matrix so that better stress transfer occurs under loading [194]. The experimental curve has been fitted with theoretical models *i.e.* modified rule of mixtures (MROM) and modified Halpin Tsai equation (***Figure 4.5b***) [121]. The Halpin Tsai equation under predicts the hardness due to the variation in the geometrical dimensions of the clay particles as well as the lower difference in hardness values of the nanoclay and polymer matrix.

Table 4.1: *Vicker hardness values for PET and P-NK nanohybrids*

Sample	Vicker Hardness
PET	11.58
P-NK1	12.13
P-NK2	12.34
P-NK4	12.48
P-NK8	13.41

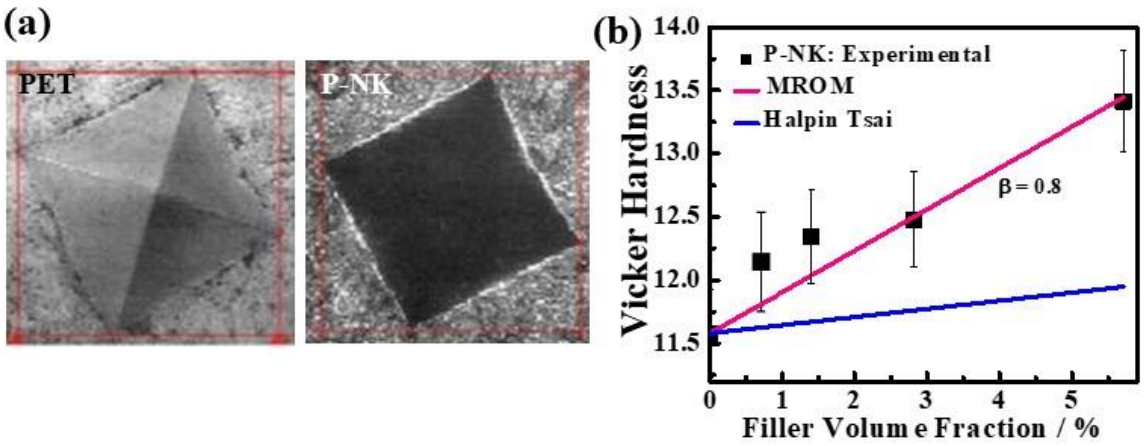

Figure 4.5: (a) *Images of impressions created by vicker hardness test; and* ***(b)*** *Experimental and predicted curves of Vicker hardness values.*

4.3.5 Temperature dependent viscoelastic properties

The storage modulus of the P-NK with 4 and 8 wt. % filler content is shown in ***Figure 4.6a***. The storage modulus of the nanohybrids increases significantly in the glassy region. In the rubbery region, especially after 75 ^{o}C, the storage modulus decreases for all the samples because of the increased chain movements at higher temperature. The storage modulus increase up to 64% for 8 wt. % filler content and 20% for 4 wt. % filler content nanohybrids at room temperature.

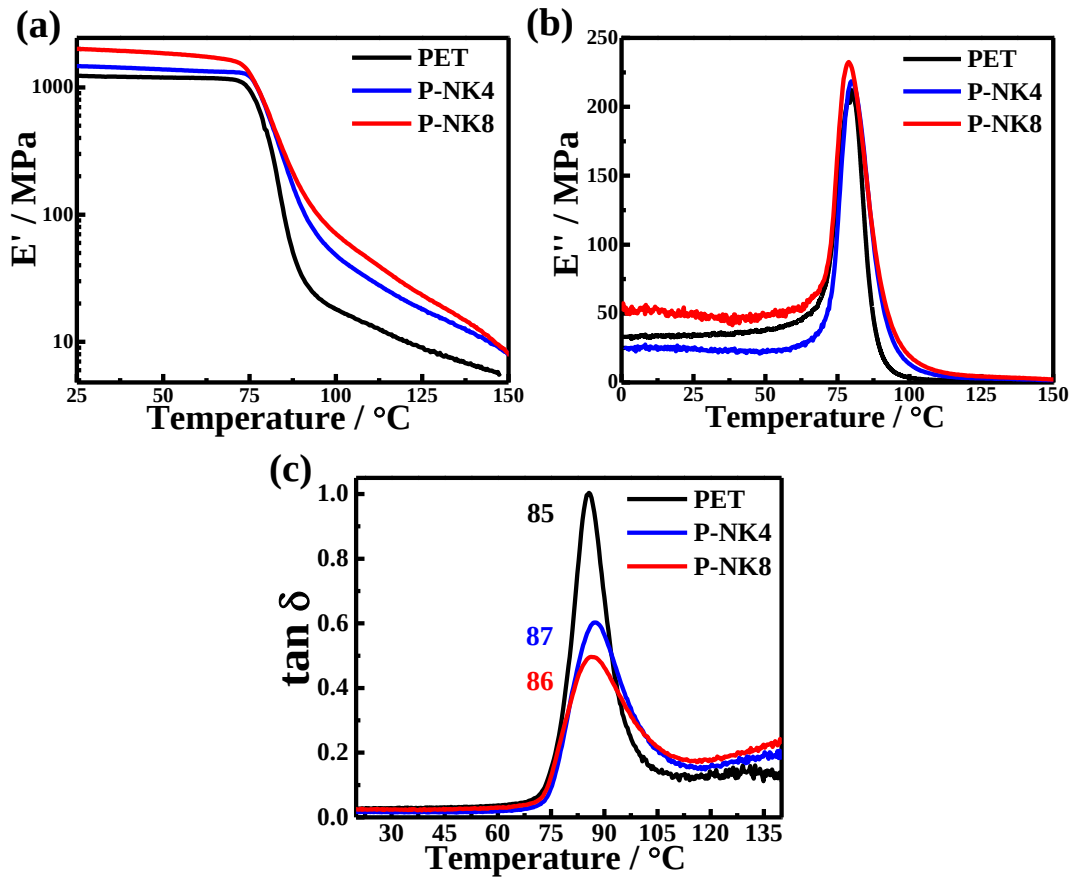

Figure 4.6: *Effect of nanoclay inclusion as measured through dynamic mechanical analyzer on* ***(a)*** *storage modulus;* ***(b)*** *loss modulus; and* ***(c)*** *tan δ of PET and its nanohybrids.*

The nanohybrids have shown improved storage modulus at room temperature in comparison to previously reported data using commercial nanoclays [206]. The presence of nanofiller imparts efficient stress transfer between the polymer matrix and the nanoplatelets and causes stiffness in the polymer matrix, hence, increases the storage modulus [233]. The loss modulus illustrates the energy lost because of the friction generated by polymer chain movements. The loss modulus increases at around the glass transition temperature as shown in ***Figure 4.6b*** which is due to decreased friction and easy movements of polymer chains in

rubbery region [234]. The loss modulus is comparatively less in nanohybrids than pristine PET. This behavior reflects the less energy loss in the nanohybrids due to the presence of the nanoplatelets. The maximum of tanδ gives the glass transition temperature (T_g). The T_g increases in presence of nanoclay as shown in ***Figure 4.6c***. The increase in glass transition temperature supports TGA and DSC analysis as shown in ***Figure 4.2*** reflecting good interactions between nanoclay and polymer matrix.

4.3.6 Effect of stretching on structure

2D-Small angle X-ray scattering

The change of structure and orientation upon stretching has been captured through 2D small angle X-ray. Both pure PET and P-NK show a well defined isotropic ring in its scattering pattern before stretching (***Figure 4.7a***). The isotropic ring in nanohybrid indicates the uniform distribution of nanoclay in the entire matrix. The stretching of samples shows a streak perpendicular to stretching direction, which indicates partial directional orientation to its randomly distributed short range order. Lorentz corrected plot of SAXS profiles are shown in ***Figure 4.7b*** where a peak appears in nanohybrids at q = 0.16 nm^{-1} which corresponds to the short range ordering of the nanoclay tactoids. The linear part of the *I(q)* vs *q* curve is fitted with Debye Bueche model to determine the correlation lengths (a_c) of the samples [173, 209]**.** The a_c of the blob of the unstretched and stretched samples are shown in ***Figure 4.7c*** which are comparable with the reported values [210]. It is evident that upon uniaxial elongation of the sample, the value of a_c has further increased.

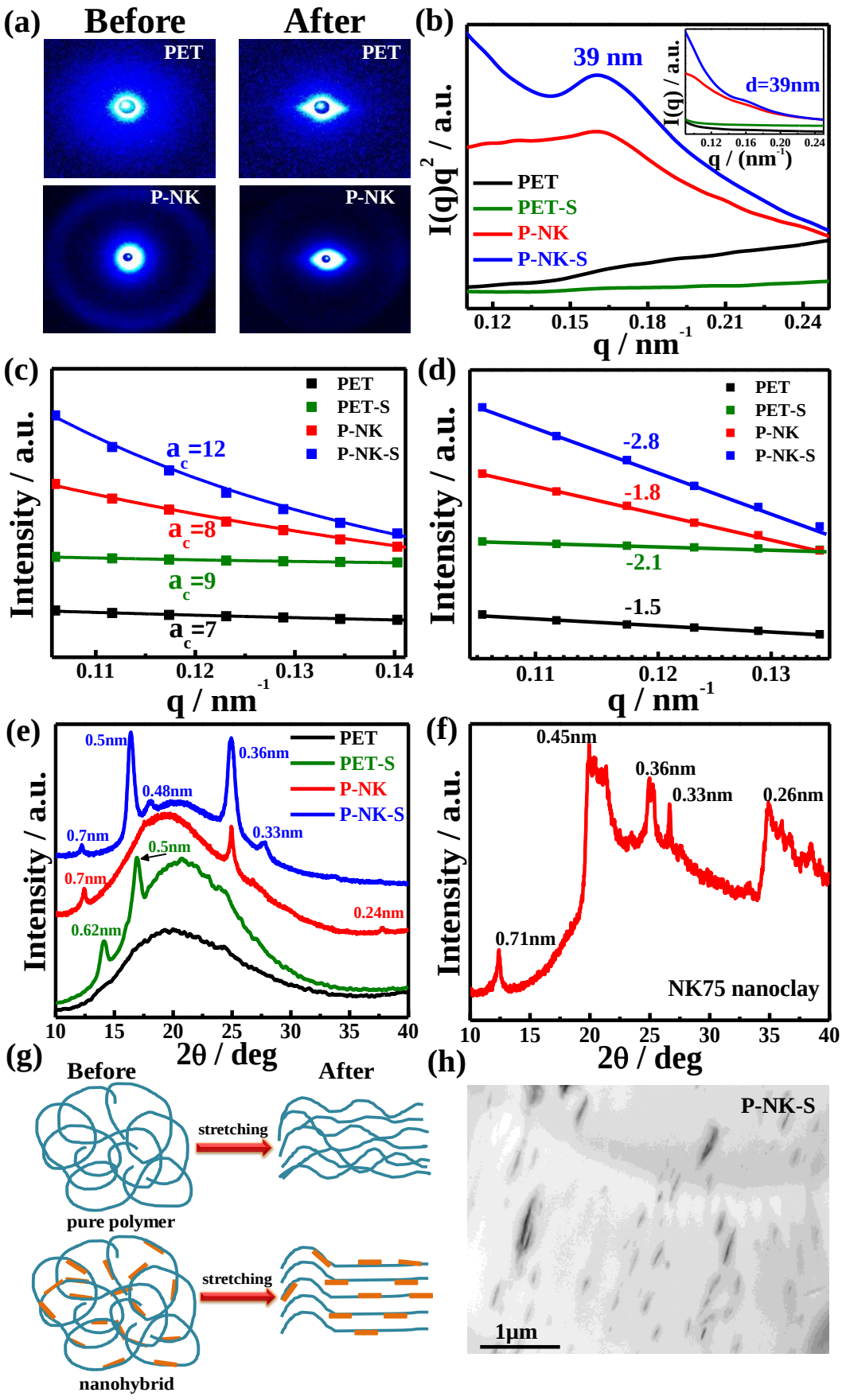
(a)
Before
After
PET
PET
P-NK
P-NK
(b)
39 nm
d=39nm
I(q) / a.u.
q / (nm-1)
I(q)q2 / a.u.
PET
PET-S
P-NK
P-NK-S
q / nm-1
(c)
Intensity / a.u.
ac=12
ac=8
ac=9
ac=7
q / nm-1
(d)
-2.8
-1.8
-2.1
-1.5
(e)
0.5nm
0.36nm
0.48nm
0.7nm
0.33nm
0.5nm
0.7nm
0.24nm
0.62nm
2θ / deg
(f)
0.45nm
0.36nm
0.33nm
0.26nm
0.71nm
NK75 nanoclay
(g)
Before
After
stretching
pure polymer
stretching
nanohybrid
(h)
P-NK-S
1μm

Figure 4.7: (a) *Small angle X-ray scattering images of indicated samples before and after stretching of PET and P-NK nanohybrid;* ***(b)*** *Lorentz corrected $I(q)q^2$ vs q SAXS profiles of the unstretched and stretched samples;* ***(c)*** *Debye-Bueche fitting (solid lines represent fitting curve) with respective correlation length (a_c) values;* ***(d)*** *Linear fit of scattering intensity versus scattering vector which shows the linear fitting curves of the intensity versus scattering vector;* ***(e)*** *Wide angle XRD patterns of the unstretched and stretched samples;* ***(f)*** *Wide angle XRD patterns of pure NK75 nanoclay;* ***(g)*** *Schematic representation of the effect of stretching showing enhanced short range molecular ordering in presence of nanoclay particle in the P-NK nanohybrid as compared with pure PET; and* ***(h)*** *TEM image of stretched P-NK nanohybrid containing 4% of nanoclay.*

On stretching the samples, the correlation length of the nanohybrid is increasing more than the pure polymer presumably due to orientation of clay platelets. The slopes of linear fit of scattering intensity versus scattering vector are also increasing in the stretched samples (***Figure 4.7d***). It is observed that the slope values for unstretched PET and P-NK are -1.5 and -1.8 while the values increase to become -2.3 and -2.8 after stretching, respectively (whereas the theoretical value for randomly oriented thin disks is -2.0 [211]). The deviation of the slope values of the experimental curves from the theoretical value can be attributed to the formation of clay tactoids or intercalated arrangement of the clay platelets. The stretched samples show the increased value of slopes because of the resulted elongation upon stretching the intercalated clay stacks. The increment of the slope values in the stretched samples is due to resulted elongation upon stretching the intercalated clay stacks.

Wide angle X-ray diffraction (WAXD)

The effect of stretching on the structural development is observed further through WAXD patterns of both the samples ***Figure 4.7e***. Pure PET shows an amorphous halo and upon

stretching, PET exhibits peaks at d-spacings of 0.62 and 0.5nm and a small hump at 0.37nm as explained in previous chapter. These sharp peaks arise due to coherency induced in the structure as an effect of stretching. WAXD pattern of P-NK shows characteristic peaks of NK75 (***Figure 4.7f***). On stretching P-NK, the intensity of the peaks enhances and few more peaks appear in the stretched P-NK. The increase in intensity of the peaks in nanohybrid is more than that of the stretched pure PET. The reason behind this behavior could be the presence of the nanoclay particle which eventually induces molecular ordering upon stretching. The PET chains adhered on the surface of the nanoclay particles get aligned along the lateral dimension of the nanoplatelets. Hence, they form a more elongated structure as compared to pure PET and this phenomenon has been shown schematically in ***Figure 4.7g***. The TEM image of stretched P-NK nanohybrid containing 4% of nanoclay shows highly oriented nanoclay platelets in the polymer matrix (***Figure 4.7h***). The platelets have also been delaminated due to stretching resulting in decrement of thickness of nanoclay stacks. Polymer chains get aligned during the stretching of nanohybrid causing delamination of clay stacks.

4.3.7 Effect of nanoclay on gas barrier

Oxygen transfer rate (OTR) through PET and its nanohybrids has been shown in ***Figure 4.8a*** and values are shown in ***Table 4.2***. OTR is found to be decreased with increasing filler concentration. Due to the homogeneous dispersion of nanoclay platelets and the strong interaction of the matrix and clay platelets, the nanohybrids acquire the improved gas barrier property. The maximum decrease of permeability value is found to be 38% for 4 wt. % filler concentration which is better than the previously reported results [94, 109]**.** It is due to the fact that nanoclay sheets block the path of gaseous molecules and force them to travel from

a longer tortuous pathway. Higher level of exfoliation and better dispersion of nanoparticles help improving the barrier properties of the nanohybrid film.

Table 4.2: *Permeability values for different concentrations of nanoclay in PET nanohybrids*

Sample	Permeability (cc.cm.m^{-2}day^{-1})
PET	0.61 ± 0.03
P-NK1	0.57 ± 0.03
P-NK2	0.51 ± 0.02
P-NK4	0.38 ± 0.01

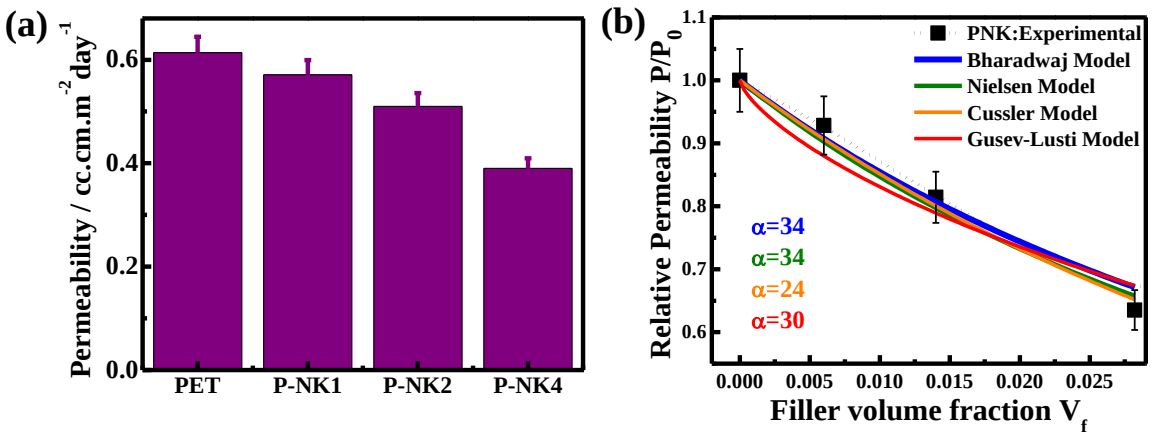

Figure 4.8: ***(a)*** *permeability reduction in P-NK nanohybrids; and* ***(b)*** *Experimental and predicted curves through different indicated models of pure PET and P-NK nanohybrid as a function of filler volume fraction at different values of aspect ratio (α).*

4.3.8 Theoretical modeling of gas permeability

The permeability data are fitted using Nielsen, Bharadwaj, Cussler and Gusev and Lusti models [215, 216, 219, 221] using aspect ratio as fitting parameter (***Figure 4.8b***). Both the models fit at an aspect ratio of 34. The value of aspect ratio obtained here is comparable to the literature reported values [94, 221, 232]. The barrier property depends mainly upon the hindrance created by the filler particles so as to force the permeate molecules to travel through a longer tortuous path. Filler particle dispersion, filler geometry and presence of

pinholes, cracks or voids play a vital role modifying the gas barrier property. In these models, tortuosity factor depends on filler volume fraction (ϕ) and aspect ratio (α) only. This theoretical fitting value of α is not equal to the values obtained by TEM images as there are many factors which play role in determining the actual value of the aspect ratio such as the intercalation level, exfoliation as well as dispersion. However, the Bharadwaj and Nielsen models fit perfectly at α = 34. Cussler and Gusev-Lusti models are also found to be fit at α = 24 and 30, respectively. Hence, gas barrier property is nicely fitted with theoretical model to explain the gas permeation required for mostly packaging applications.

In brief, NK75 nanoclay has profound effect on mechanical, thermal and gas barrier properties of PET nanohybrid as compared to commercially available clay. The reasons of improved properties are explained from microstructural point of view along with the theoretical prediction of property enhancement using various models. The effect of uniaxial elongation on structure has also been elucidated.

4.4 Conclusion

The nanohybrids of PET have been prepared through solvent casting route. Nanoclay has found to be homogeneously dispersed and intercalated. The nanohybrids have showed better mechanical properties where modulus have found to be increased 66% for 8% clay loading whereas toughness has been found to be comparable to the PET. Various models have been used to predict the modulus closely. Vicker hardness of the nanohybrids has been found to be increasing with filler loading (up to 16%). Effect of stretching has been extensively studied through SAXS and WAXS. Orientational ordering has been increased upon stretching and it further increased in nanohybrids. The gas barrier property of nanohybrids

has been improved (38% for 4% filler). The precise prediction has been done using different models. A balance among the gas barrier, mechanical and thermal properties have been achieved using NK75 nanoclay whose values are considerably better than commercially available fillers.